

# Current transport mechanism in Au-*p*-MgO-Ni Schottky device designed for microwave sensing

A. F. QASRAWI<sup>a,c,\*</sup>, H. K. KHANFAR<sup>b</sup>

<sup>a</sup>Department of Physics, Arab-American University, Jenin, Palestine

<sup>b</sup>Department of Telecommunication Engineering, Arab-American University, Jenin, Palestine

<sup>c</sup>Group of Physics, Faculty of Engineering, Atilim University, 06836 Ankara, Turkey

Au/MgO/Ni back to back Schottky tunnelling barriers are designed on the surface of an MgO thin layer and are electrically characterized. The current voltage curve analysis has shown that thermionic emission, field effect thermionic (FET) emission and space charge limited current are dominant transport mechanism in distinct biasing regions. It was shown that, while the device is reverse biased with voltages less than 0.31 V, it conducts by tunnelling (FET) through an energy barrier of 0.88 eV with a depletion region width of 15.7 nm. As the voltage exceeds 0.46 V, the tunnelling energy barrier is lowered to 0.76 eV and the depletion region widens and arrives at the reach-through running mode. The device was tested in the microwave electromagnetic power range that extends from Bluetooth to WLAN radiation levels at oscillating frequencies of 0.5 and 2.9 GHz. In addition, a low power resonating signal that suits mobile data is superimposed in the device. It was observed that the Au/MgO/Au sensors exhibit a wide tunability range via voltage biasing or via frequency control. The signal quality factor is  $3.53 \times 10^3$  at 2.9 GHz. These properties reflect applicability in microwave technology as wireless and connectorized microwave amplifiers, microwave resonators and mixers.

(Received April 24, 2015; accepted August 3, 2016)

**Keywords:** Shottky, MgO, Sensors, Barrier height, Microwave, Mobile

## 1. Introduction

Metal-semiconductor-metal (MSM) junctions are now attracting the attention of electronic device designers due to their remarkable role in electronics and optoelectronics [1-3]. They are used in optical communications as photodetectors. MSM photodetectors are used as optical inter-connectors, due to their performance in high speed operations and their applicability to construct 2D detector arrays. Such type of photodetectors had been extensively used for wavelengths ranging from ultraviolet to infrared and they are reported [3] to be capable of performing at extremely high speed data rates (greater than 30 GHz for crystalline Si and greater than 290 GHz for bulk GaAs substrates). MSM devices made of  $Al_xGa_{1-x}N$  with Ni Schottky contacts are reported to exhibit novel properties for pressure sensing [4]. SMS structures also find applications as a selection device for memory cells [5].

Recently, V. I. Shashkin [6], reported the characteristics of new sensing elements based on symmetrical metal-semiconductor-metal structure which were designed for the detection of microwave-terahertz signals. The new structure reflected characteristics that exceed in some cases similar characteristics of the detector zero-bias diodes. In another work, an integrated Schottky MSM photodetectors made of GaAs in the central strip of coplanar lines for microwave switching applications was also designed [7]. The MSM photodetectors in the microwave lines reflected an active surface of  $3 \times 3 \mu m^2$  and electrode spacing of 0.2, 0.3, 0.5 and 1  $\mu m$ . The characterization of the structures in darkness and

under illumination revealed an "On/Off" ratio of 26–28 dB at 20 GHz and 25 GHz. Such results demonstrated that the MSM structures can display a good performance for microwave photoswitching.

In the scope of the above reported important applications of MSM devices, here in this article, we will discuss and analyze the main physical parameters of a new type of MSM device made of Au and Ni metals on magnesium oxide (MgO) layer. The Au/MgO/Ni device is recently reported to exhibit a photovoltaic effect presented by an open circuit voltage of 0.12-0.47 V, short circuit current density of 3.9-10.5  $\mu A/cm^2$ , quantum efficiency of 0.662-0.052, and responsivity of 0.179-0.024 A/W under photoexcitation optical power of 2.2- 28.2  $\mu W$  is observed [2, 8]. Pei-Nan Ni et al. employed the Au/MgO interface as a top interface for fabricating bias-polarity dependent ultraviolet/visible switchable light-emitting device. The device exhibited emission bands that can be switched from the ultraviolet region to the orange region through changing the polarity of the applied bias [9]. In the current study, we will report and discuss the properties of Au-*p*-MgO-Ni device structure based on metal-semiconductor-metal geometrical design. Such devices usually find applications as frequency mixers, amplifiers and monostable-bistable circuit elements (MOBILE), microwave photoswitches and photoacoustic signal readers [6-10]. The traditional MOBILE uses two resonant tunnelling diodes connected in series and driven by an oscillating bias voltage to produce monostable-bistable transition of the circuit [11]. The monostable means that the circuit always comes to rest in one position

only, while bistable means that it may come to rest either in one of two positions. Magnesium oxide is a material which exhibit a p- type of conduction with a work function of ( $\phi_{MgO}$ ) 5.76 eV [8], as a result, it exhibits a Schottky type of barriers with most metals that have work functions less than 5.76 eV. Thus, here in this design we will use two different types of metals with close work functions as contact points on the surface of MgO to establish a tunnelling barrier. The need for tunnelling barrier at least on one side of the device is to construct a region that leads to a resonant circuit at particular voltages. The other side of the device is to work in such a way that it keeps the dark current minimum to guarantee passive mode running of the device with high speed responsivity. The two metals were experimentally found to be Au and Ni. They exhibit work functions of  $\sim 5.40$  and  $\sim 5.35$  eV [12], respectively. Practically, there should be no important difference between the Au and Ni metals in the metal-semiconductor device production. However, one may prefer to use the Au metal, as it is more resistant to corrosion and moisture and may prefer Ni as it is cheaper than Au. Our experimental trails has shown that the Au contact exhibit stronger bonding properties on the surface of MgO than Ni. Here, we will focus on the current –voltage characteristics and we will investigate the dominant current conduction mechanism during the forward and reverse direction. In addition, an ac signal of gigahertz frequency will be superimposed into the device and the output signal will be analyzed to reveal the device responsivity.

## 2. Materials and methods

The preparation method of these films was previously described [2]. The conduction nature of MgO was tested by the hot probe technique. Two different Au and Ni metal (in paste form) contacts of high purity were painted on the surface of the MgO layer. The surface was masked before metallic painting. The layer thickness of the MgO was  $\sim 100$   $\mu\text{m}$ . The distance between the Ni and Au electrodes was 300  $\mu\text{m}$  and the area of each of the Ni and Au contacts was  $\sim 270$   $\mu\text{m}^2$ . The  $I$ - $V$  curve was registered between gold and Nickel contacts (inset of Fig. 1). The dc current-voltage ( $I$ - $V$ ) characteristics were carried out using computerized Keithley 230 voltage source and Keithley 6485 picoammeter. The data were transferred using Keithley high-quality low-noise coaxial cables to reduce external effects. The differential resistance of the device was recorded with respect to a reference resistance. A dc resistance value was fixed to allow the observation of the differential resistance associated with the imposed ac signal. In this process an ac signal of 0.5 V and 2.9 GHz was imposed into the devices. The applied ac signal amplitude was less than the dc voltage used to set the reference. The changes in the resistances as a function of applied voltage were then monitored. The ac signal was provided by Agilent N9310A RF Signal Generator (9 kHz - 3 GHz). The signal power was recorded with the help of GSP-830 3.0 GHz spectrum analyzer. The data were carried with high quality cables which were kept as short

as possible. All the measurements were carried in the dark at room temperature in natural room atmosphere and the devices were not isolated from the environment. The reproduction of the results was tested at different times to ensure the results consistency.

## 3. Results and discussion

The geometrical design of the Au/MgO/Ni MSM device is shown in the inset of Fig. 1(a). The same figure reflects the current ( $I$ ) -voltage ( $V$ ) characteristics of the device under test (DUT) being registered at room temperature. The MSM device works on the principle that at the instant one junction is forward biased, the other junction is reverse biased. Thus, in the forthcoming analysis the Au contact side will represent the forward biasing ( $I_{Au}=I_F$ ) and the Ni contact will represent the reverse biasing ( $I_{Ni}=I_R$ ).

The  $I$ - $V$  characteristics of the DUT reflect a biasing dependent rectification ratio that increases from 1.2 at 1.0 V to 1.5 at 2.7 V and reaches 4.0 at 3.0 V. The weak rectification ratio is ascribed to blocking of the forward current by the reverse current, which is generated from the Ni-contacted side of the DUT. In order to investigate the details of the current transport mechanism in this device, the logarithm of the  $I$ - $V$  curve of the forward and reverse currents are re-plotted in Fig. 1(b) and (c), respectively. As Fig. 1(b) shows the forward current –voltage dependence reflects three regions of conduction mechanism. The Ohmic ( $I \propto V^{1.0}$ ) region which dominates in the applied voltage range of 0.1-0.80 V, the tunnelling ( $I \propto V^{0.6}$ ) in the region of 0.81-1.97 V, and the space charge limited ( $I \propto V^{2.0}$ ) in the range of 1.98-2.64 V. For higher applied voltages, the current abnormally increases following higher degree of voltage dependency. On the other hand, the reverse bias characteristics shown in Fig. 1(c), reflects a  $I \propto V^{0.6}$  dependence in the range of 0.09-0.57 V. For reverse biasing voltages greater than 0.57 V and less than 1.23 V,  $I$  is  $V^{0.3}$ . In the range of 1.25-2.02 V,  $I \propto V^{1.0}$  and  $I \propto V^{3.1}$  for higher applied voltages. Generally, the dependence of the current on the square root of the voltage indicates an electric field assisted tunneling current transport mechanism in the device in which the current is given by, the Poole–Frenkel and/or Richardson-Schottky effects. The Poole–Frenkel mechanism usually arises from the electric-field-assisted thermal excitation of charge carriers from charged/neutral traps or impurity sites into the semiconductor energy band. This internal emission can transfer charges from potential traps at impurity levels to the conduction band. In this process, electric field assisted Coulomb potential type donor traps lowers the potential and support detrapping. In the Poole-Frenkel effect, electrons first neutralizing the trap will jump to the next trap causing a net flow of electrons [13, 14]. On the other hand, the Richardson–Schottky effect is a field-assisted thermionic emission of charge carriers injected from metal electrodes into the semiconductor over a potential barrier.

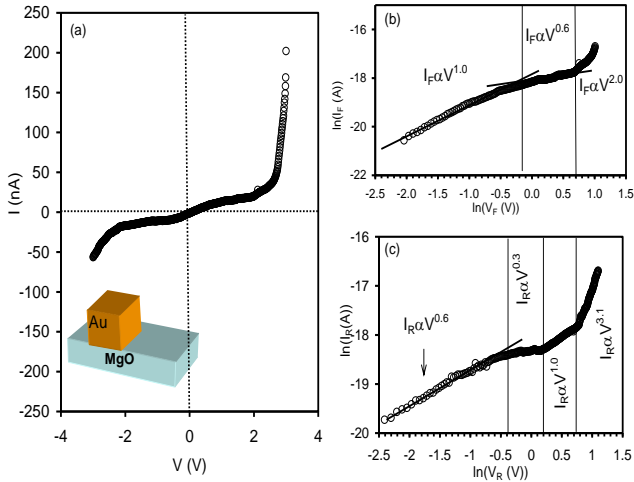


Fig. 1. (a) The current voltage characteristics and geometrical design of Au/MgO/Ni MSM device. (b) the logarithmic plot of the forward current-voltage characteristics. (c) the logarithmic plot of the reverse current-voltage characteristics.

The current–voltage behaviour for the Richardson–Schottky/Poole–Frenkel effect is given by,

$$I = AA^{**}T^2V^\gamma \exp(-q\Phi/kT) \quad (1)$$

$$\Phi = \phi_0 - n \left( \frac{q\eta}{4\pi\epsilon_0\epsilon_r} \right)^{1/2} \frac{1}{\sqrt{w}} \sqrt{V} \quad (2)$$

here,  $\Phi$  is the field-dependent activation energy that represents a Schottky-barrier height or trapping/donor-site energy in the electric field,  $\phi_0$  is the no field value,  $\epsilon_r$  is optical dielectric constant of the material,  $A = 0.027 \text{ cm}^2$  is the device area,  $A^{**}$  is Richardson constant and  $w$  the effective width of the interfacial depletion region. The pre-factor of  $\sqrt{V}$  shown in eq. 2 is the Poole Frenkel coefficient ( $\beta_{PF}$ ) or  $\beta_S/\sqrt{w}$  is the Richardson-Schottky coefficient ( $\beta_{PF} = 2\beta_S$ ). For the Schottky-emission mechanism,  $n = \eta = 1$ ,  $\gamma = 0$ . For a modified Poole–Frenkel mechanism,  $n = 2$ ,  $\eta = 1$  or  $2$ ,  $\gamma = 1$ ,  $\phi_0 = E_0$  centre-field trapping centre energy) [14]. Both of the Poole-Frenkel and Richardson-Schottky conduction mechanisms are tested for the reverse biasing case. However, because the plot of  $\ln(I_R/V_R) - \sqrt{V_R}$  (the subscript R denotes for reverse biased condition) which is illustrated in the inset of Fig. 2 is not linearly increasing as supposed, the Poole-Frenkel current conduction mechanism appears to be not dominant for low applied voltages ( $3kT < V < 1.6 \text{ V}$ ). On the other hand, the plot of  $\ln(I_R) - \sqrt{V_R}$  shown in Fig. 2 reveals a linearly increasing plot over the same studied range of voltage. The slope and intercept of the linear plot presented by solid line in Fig. 2 leads to the calculation of the device

parameters and indicates that the current conduction mechanism is governed by the Richardson-Schottky mechanism in which charge carriers are injected from (high concentration region) metal to (low concentration region) semiconductor by electric field assisted thermionic emission (tunnelling).

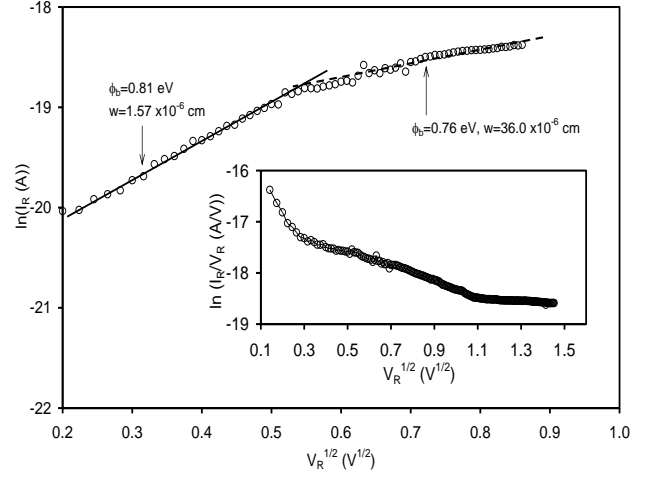


Fig. 2. The  $\ln(I_R) - \sqrt{V}$  dependence for the DUT.

The inset displays the  $\ln(I_R/V) - \sqrt{V}$  dependence.

The Richardson constant  $A^{**} = 120 \text{ m}^*$  is determined as 48.16 assuming an effective mass of  $m^* = 0.4 m_0$  [14]. By substituting the temperature ( $T$ ) as 300 K and using the intercept of the solid line shown in Fig. 2, the Richardson–Schottky barrier height ( $\phi_b$ ) to the charge flow was determined as 0.81 eV. On the other hand, the slope of the same solid line allowed the calculation of the effective barrier width as  $w = 1.54 \times 10^{-5} / \epsilon_r \text{ cm}$ . The value of the optical static dielectric constant for MgO is reported as 9.83 [15]. Using this value, the width of the interfacial region,  $w$ , turns out to be  $1.57 \times 10^{-6} \text{ cm}$ . In the voltage range of 0.46–0.73 V, shown by dashed line in Fig. 2, the same calculations reveal a barrier height of 0.76 eV and a depletion region width of  $36.0 \times 10^{-6} \text{ cm}$ . The depletion layer width of MSM device is given by [16]

$$W_{D1} = \sqrt{\frac{2\epsilon_s}{qN_A}(V_{bi} - V_1)} \quad \text{and} \quad (3)$$

$$W_{D2} = \sqrt{\frac{2\epsilon_s}{qN_A}(V_{bi} + V_2)} \quad (4)$$

where  $W_{D1}$  and  $W_{D2}$ , are the depletion widths in the p-layer for the reverse- and forward-biased barriers, respectively;  $V_1$ , and  $V_2$ , are the fraction of the applied voltage developed across the respective junctions,  $N_A$  is the ionized impurity density; and  $V_{bi}$  is the built-in potential. For p-type MgO of holes mobility of  $10 \text{ cm}^2/\text{V}\cdot\text{s}$ ,

assuming an ionized impurity density of  $\sim 10^{16} \text{ cm}^{-3}$  in MgO (experimentally determined) and using eq. (3) for the reverse biasing case, one may obtain a built in voltage – fractional voltage difference of 2.26 meV when applying voltages less than 0.31 V and 1.19 V when applying voltages greater than 0.46 V.

Recalling that the current is the sum of the forward saturation current (of a Schottky diode with a barrier height  $\phi_{bp}$ ), generation-recombination current, and surface leakage current. Thus, further increase in the

$$V_{RT} \approx \frac{qN_A W^2}{2\epsilon_s} - W \sqrt{\frac{2qN_A V_{bi}}{\epsilon_s}} = V_{FB} - W \sqrt{\frac{2qN_A V_{bi}}{\epsilon_s}} = (1.19 - 2.18\sqrt{V_{bi}})_{W=36 \times 10^{-6} \text{ cm}} \quad (5)$$

When the applied reverse voltage is equal or greater than the built in voltage, the flat band condition ( $V_{bi} = V_1$ ) is satisfied and the flat band (the energy band at the positively biased contact (Au -side)) voltage  $V_{FB}$  is given by eq. (5). The significance of  $V_{RT}$  appears when the MSM device is run at dc voltage and microwave frequencies. In the region of  $V_{RT} < V < V_{FB}$ , the hole forward current dominate overcoming the barrier and leading to an exponential increase in the current values with increasing voltages. In addition, in a reverse bias application, the depletion width of the junction is increased, thus effectively reducing the junction capacitance and increasing the response speed.

In the scope of this recall, one may explain the reverse current -voltage characteristics as follows; for applied reverse voltages in the range of  $0 < V_R < 0.31 \text{ V}$ , the diode is normally running within a depletion region width of  $1.57 \times 10^{-6} \text{ cm}$  and barrier height of 0.81 eV. This energy barrier is very narrow as its width is 15.7 nm. The narrow barrier makes the charge transport via tunnelling process preferable. In this case, the current conduction mechanism is governed by electric field assisted tunnelling of charged particles through the narrow barrier. As the voltage becomes more negative  $V < 0.31 \text{ V}$ , the current which is still dominated by the tunnelling of charge carriers through a potential barrier of 0.76 eV, arrives at the reach-through condition with the depletion region width of  $36 \times 10^{-6} \text{ cm}$  and with  $V_{bi} - V_1 = 1.19 \text{ V}$ . When the applied reverse voltage exceeds 0.73 V, the very weak current-voltage dependence ( $I \propto V^{0.3}$ ) is then due to exceeding of reach-through voltage. When  $V_{RT}$  is reached the hole current

$$(I_p = AA_p^{**} T^2 \exp\left(-\frac{q(\phi_{bp} + V_{bi})}{kT}\right) \left(\exp\left(\frac{qV_1}{kT}\right) - 1\right))$$

which conducts by thermionic emission over a barrier height of  $\phi_{bp} = 0.76 \text{ eV}$  become the dominant current [16], in this situation the current exponentially increases with applied voltage however, this mechanism is also influenced by the effect of generation –recombination,

reverse voltage forces the forward -biased depletion region to eventually reach through to the reversed-biased depletion region and now,  $w_{D1} + w_{D2} = W$ . The corresponding voltage which is known as the reach-through voltage  $V_{RT}$  is obtained from the condition that  $W = W_{D1} + W_{D2}$  which is the length of the p region through the relation,

avalanche breaks down and image force lowering potentials processes [16]. Thus, for all applied voltages greater than 1.19 V (see Fig. 1(c) -forth region),  $I \propto V^{3.1}$  or  $I \propto \exp(0.51V)$  (in the range of 1.20-2.22 V) and  $I \propto \exp(1.32V)$  above 2.23 V.

It is worth notifying that, when the same above mentioned analysis are repeated for the forward biased side (Au-side) through the plots of  $\ln(I_F) - V^{1/2}$ , The barrier height and depletion layer width display values of 0.82 eV and  $8.14 \times 10^{-6} \text{ cm}$ , respectively, in the applied voltage region of 0.8-2.0 V. The value of the barrier height being 0.82 eV indicate that the device under test work under symmetrical conditions. This behaviour is expected because the difference in the work function of metals is just 0.05 eV.

For the ability of microwave oscillating, the applied voltage at the Au/MgO/Ni device terminals must be greater than  $V_{RT}$  and less than  $V_{FB}$ . As eq. 5 indicates, the  $V_{RT} = V_{FB}$  condition is satisfied at  $V_{bi} = 0.30 \text{ V}$ . Thus, for all the reverse biasing voltages greater than 0.73 V (the limit at which we were able to determine the  $W_{D1}$  value or the reach through position), a microwave resonant circuit construction is possible. Fig. 3(a) illustrates the results of the resistance variation as function of power of a 0.5 GHz ac signal being varied in the range that extends from Bluetooth (0.0 dBm) to the wireless local area network power levels (WLAN) (20 dBm). The applied reverse dc voltages (2.0, 4.0 and 6.0 V) were greater than  $V_{RT}$ . The figure also displays the resistance of the device as a response to a 2.9 GHz oscillating signal being superimposed on a 4.0 V dc reverse biased DUT. One remarkable point is that, the greater the reverse dc biasing the lower the resistance value. Namely, at 20 dBm, for example, the resistance exhibit values of 11.48, 2.90 and 2.44  $M\Omega$  for biasing voltages of 2, 4 and 6 V, respectively. The decrease in the resistance is due to the generation of high currents associated with voltage biasing. When the biasing voltage is fixed at 4.0 V and the frequency is changed from 0.5 GHz to 2.9 GHz, the resistance exhibited value of 3.54 at 20 dBm (2.2 V). The numerical data reflect the wide tunability of the device under microwave oscillating frequencies and under the dc

biasing effects. Such properties make the device promising to be used in microwave applications as frequency mixers, amplifiers and monostable-bistable circuit elements (MOBILE). As an additional test which confirms the device suitability for the third generation of mobiles 3G/UTMS, the Au/MgO/Ni device was inserted as microwave resonator and subjected to ac signal of amplitude that is shown as reference in Fig. 3(b). The signal frequency was 2.9 GHz. There was no dc biasing for the DUT. The input to the device terminals is shown by the dashed line in Fig. 3(b) and the output signal is shown by the solid line. As it is clearly observable, the output power at maximum peak level is 80% of the incident one. Although the incident power was of very low level that suits the arriving signals at mobile amplifiers, the output signal is still in the same range. It is clearly seen from the Fig. 3(b) that the DUT is capable of signal oscillating even at  $\sim -100$  dBm ( $2.2 \mu\text{V}$ ) level. In addition, the quality factor ( $Q = \Delta f / f$ ) for the 2.9 GHz signal presented in the figure is determined as  $3.53 \times 10^3$ .

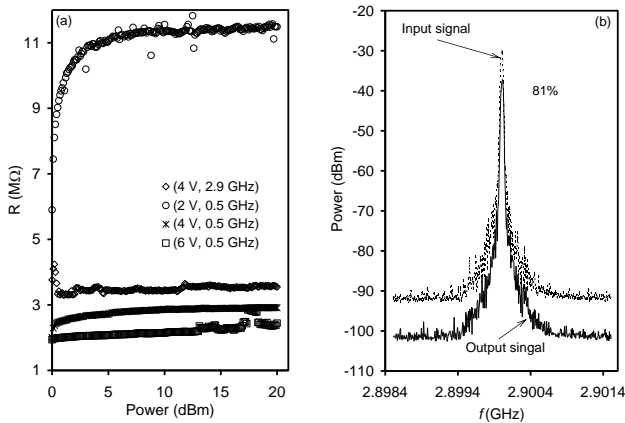


Fig. 3. (a) The resistance of the Au/MgO/Ni as function of ac power. (b) The device response to an oscillating signal at 2.9 GHz.

As a complementary work we now turn our attention to the Au contacted side of the device in which the DUT is forward biased. The I-V characteristic of the device is represented on a logarithmic scale in Fig. 1(b). As previously mentioned, the conduction is governed by thermionic emission (Ohmic), tunnelling and space charge limited conduction mechanisms. Based on thermionic emission theory which considers the device series resistance effects on the device ideality factor and barrier height and using the equations described in reference 16 [17], the derivative of  $dV/d(\ln(I))$  were evaluated and presented as a function of  $I$  in the inset of Fig. 4. The slope and the intercept of the solid line shown in the inset revealed an ideality factor and series resistance of 1.28 and  $53 \text{ M}\Omega$ , respectively. Using these data Cheung's function,  $H(I)$ , was evaluated and plotted in Fig. 4. The intercept of the solid line which is shown in

the figure allowed determining the forward bias barrier height as 0.88 eV.

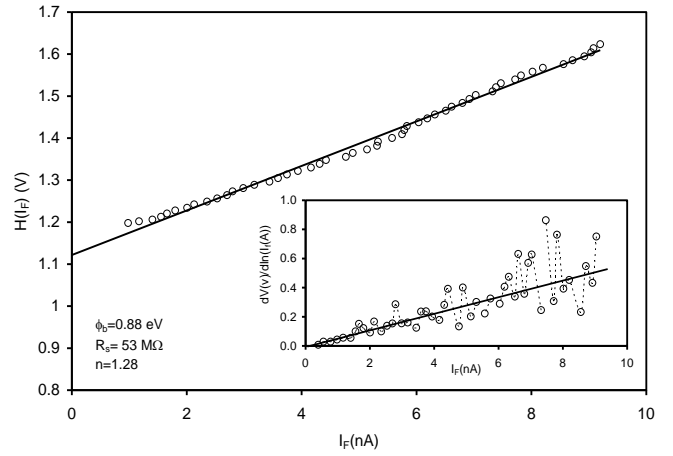


Fig. 4. The Cheung function  $H(I)$  plot for the device under forward biasing condition. The inset displays the  $dV/d\ln(I) - I$  for the DUT.

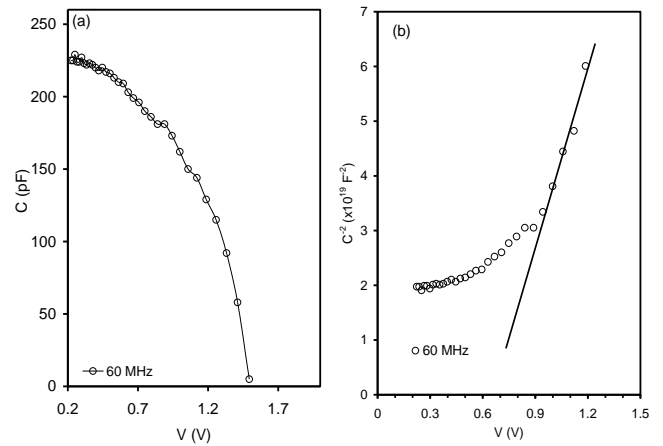


Fig. 5. (a) The capacitance ( $C$ )-voltage ( $V$ ) characteristics at 60 MHz. (b) the  $C^{-2}$ - $V$  plot.

On the other hand, Fig. 5 displays the capacitance ( $C$ )-voltage ( $V$ ) characteristics of the device being recorded at frequencies ( $f$ ) of 60 MHz. The data which are illustrated in Fig. 5 (a) show a drastically falling capacitance values via increasing applied voltage. The decreasing trend becomes more pronounced as the applied voltage exceeds 0.4 V and it reaches zero value at the inversion point where  $V_a$  is comparable to 1.19 V. The  $C$ - $V$  data which was analyzed by plotting  $C^{-2} - V$  characteristics as in Fig. 5 (b) and revealing the slopes of the trends allowed determining the density of non-compensating carriers ( $N_i$ ) as  $2.35 \times 10^{14} \text{ cm}^{-3}$  and the barrier height ( $\phi_{(C-V)}$ ) as 0.87 eV in the applied voltage range of 0.89-1.20 V. This value, approximately, coincides with that which was obtained as 0.88 eV using Cheung's function method. The latter value is slightly higher than

we have calculated from the reverse bias analysis. The difference may be attributed to the difference in the Au and Ni work functions in addition to other reasons like device internal series resistance effect which cause a particular voltage drop, the induced defects, electron-hole pair recombination and image force effects [16] and Schottky barrier inhomogeneities. The inhomogeneities are possibly originating from the structural dislocations, the grain boundaries, and the structure-dependent interface dipoles that are created at the metal-semiconductor interface [18].

#### 4. Conclusions

In this study, the electrical properties of the Au/MgO/Ni device were investigated in details. The MSM device exhibit barrier heights of 0.76 and 0.88 eV at the Ni-MgO and Au -MgO interfaces respectively. The device ideality factor was found to be 1.28. Generally both of the forward and reversed contacts exhibit a field assisted thermionic emission current transport characteristics. The device technological applicability was tested under microwave frequencies of 0.5 and 2.9 GHz. It is observed that the device resistance can be altered from 11 -2.2 MHz by changing the dc biasing voltage. In addition, the DUT was found to be able to screen very weak microwave signals that suits mobile amplifiers.

#### Acknowledgement

The authors would like to acknowledge and submit thanks to the scientific research council at the ministry of high education of the state of Palestine for their support through the project coded 2/1/2013. Thanks also go to scientific research committee members at the Arab American University for their financial support and encouragements. This research was partially funded by the AAUJ research deanship through the first cycle of 2013.

#### References

- [1] L. C. Yang, R. X. Wang, S. J. Xu, Z. Xing, Y. M. Fan, X. S. Shi, K. Fu, and B. S. Zhang, *J. Appl. Phys.* **113**, 084501 (2013).
- [2] H. K. Khanfar, A. F. Qasrawi, *Mater. Sci. Semicond. Proc.* **29**, 183 (2015).
- [3] F. Haas, M. Etal-Sem I. Ductor: Metal Photodetectors For Optical Interconnect Applications, RL-TR-96-217 In-House Report, Rome Laboratory Air Force Materiel Command Rome, New York, 1997.
- [4] Z. Hassan, Y. C. Lee, S. S. Ng, F. K. Yam, Y. Liu, Z. Rang, M. Z. Kauser, P. P. Ruden, M. I. Nathan, *phys. Stat. sol. (c)* **3**, 2287 (2006).
- [5] D. H. Wells, B. Srinivasan, J. K. Zahurak, US patent No: US 2013/0069028 A1, (2013).
- [6] V. I. Shashkin, *IEEE J. Electron Dev. Soc.* **1**, 76 (2013).
- [7] A. D. Zebentout, Ab. K. Aissat, Z. Bensaad, M. Zegaoui, A. Pagies, D. Decoster, *Optics & Laser Technol.* **47**, 1 (2013).
- [8] A.F. Qasrawi, *Mat. Sci. Eng. B*, **178**, 851 (2013).
- [9] P. N. Ni, C. X. Shan, B. H. Li, S. P. Wang, D. Z. Shen, *ACS applied mater. & interfaces* **6**, 8257 (2014).
- [10] M. Murakami, N. Takabatake, K. Sato, T. Arai, *Electron. Commun. Jap.*, **96**, 65 (2013).
- [11] K. Gan, J. Tsai, C. Hsian, Y. Li, W. Yeh, *Analog Integr. Circ. Sig. Process.*, **68**, 379 (2011).
- [12] H. L. Skriver, N. M. Rosengaard, *Phys. Rev. B*, **46**, 7157 (1992).
- [13] M. M. A. Jafar, *Semicond. Sci. Technol.* **18**, 7 (2003).
- [14] W. H. Butler, X.-G. Zhang, T. C. Schulthess, *Phys. Rev. B*, **63**, 054416 (2001).
- [15] A. R. Oganov, M. J. Gillan, G. D. Price, *J. Chem. Phys.* **118**, 10174 (2003).
- [16] S. M. Sze, *Physics of Semiconductor Devices*, Wiley & Sons, New Jersey, 2007.
- [17] A. F. Qasrawi, S. M. S. Elayyat, N. M. Gasanly, *Cryst. Res. Technol.* **47**, 615 (2012).
- [18] Sh. Shivaraman, L. H. Herman, F. Rana, J. Park, M. G. Spencer, *Appl. Phys. Lett.* **100**, 183112 (2012).

---

\*Corresponding author: atef.qasrawi@atilim.edu.tr  
atef.qasrawi@aaui.edu